



Characterization of material flow in friction stir-assisted incremental forming with synchronous bonding of dissimilar sheet metals

Renhao Wu^{1,2} · Meng Li^{1,2} · Xinmei Liu^{1,2} · Sheng Cai^{1,2} · Jun Chen^{1,2}

Received: 3 March 2020 / Accepted: 17 July 2020 / Published online: 2 August 2020
© Springer-Verlag London Ltd., part of Springer Nature 2020

Abstract

Material flow is evaluated to investigate the mechanism of pin-less friction stir-assisted incremental forming with synchronous bonding (FS-ISF&SB) process in a macro and micro scope. Dissimilar metal sheets AA5052-H32 and DC05 are incrementally formed with synchronously bonding by this novel process. Analytical mechanical models combined with microscopic image reveal that materials experience severe but different flow modes during the process. To make clear the underlying forming mechanism, the fabricated part is divided into three zones: wall flow zone (WFZ), rotation flow zone (RFZ), and bump structure flow zone (BSFZ). Bonding may even appear at Fe-Al interface to produce Fe-Al intermetallic compound in WFZ and RFZ, which depends on uncoordinated deformation controlled by mechanical force coupled with heat. Contributed to the torque transfer applied by forming tool, obvious wall side deflection in WFZ and grain refinement at the near surface area in RFZ are observed. Based on the simulation characterization, thermal effect is considered to build force frame on the deformation element for making semi-quantitative investigation of softening effect on BSFZ. This work prompts a better understanding of the underlying mechanism of this process and establishing the process window for potential industrial applications.

Keywords Material flow · Dissimilar bonding · Incremental forming · Pin-less friction stir · Macro-microscopic mechanism

Nomenclature

Δh	Step down (mm)	t_U, t_L	Current thickness of upper and lower layer (mm)
μ	Coefficient of friction	k, n	Coefficient in material hardening rule
v	Feed rate (mm/s)	K, n	Coefficients in Hollomon material hardening rule
ω	Forming tool rotation speed (rpm)	r_h	Part radius at current height (mm)
ε	Equivalent plastic strain	σ	Equivalent stress (MPa)
T_r	Room temperature (°C)	θ	Circumferential contact angle (°)
R_t	Tool radius (mm)	t_0	Initial sheet thickness (mm)
T_{melt}	Material melting temperature (°C)	σ_s	Yield stress (MPa)
$\varepsilon_t, \varepsilon_\varphi, \varepsilon_\theta$	Strain in thickness, tangential, and circumferential directions	β	Forming angle (°)
$\sigma_t, \sigma_\varphi, \sigma_\theta$	Normal stress in thickness, tangential, circumferential directions, and shear stress (MPa)	R_d	Designed maximum opening radius of part (mm)
		σ_{tb}	Boundary stress in thickness direction (MPa)

✉ Jun Chen
jun_chen@sjtu.edu.cn

¹ Department of Plasticity Technology, School of Materials Science and Engineering, Shanghai Jiao Tong University, Shanghai 200030, China

² National Engineering Research Center of Die & Mold CAD, School of Materials Science and Engineering, Shanghai Jiao Tong University, Shanghai 200030, China

1 Introduction

Sheet metals have been widely used in automotive, aerospace, and aircraft industrial productions for decades. With the continually increasing demand of environmental-friendly and higher material performance in practical application, relevant challenging material and more complex processing

technology are required with urgent solutions. As for the aspect of materials, laminates tend to replace single metal layer for overcoming the drawbacks of the limited sole property. Dissimilar metal laminate is a potential material fabricated by layered joining method [1]. In addition, the laminates can save rare materials, reduce product cost, and show better engineering performance. Therefore, Al/steel bimetal hybrid structures are widely used, in which aluminum alloy can effectively improve the corrosion resistance and thermal conductivity and reduce specific gravity of steel, while steel can effectively improve the strength and mechanics performance of composite materials. At present, the manufacturing method of the laminates is to form a flat plate of a multi-layer material by rolling [2], explosion [3], hot dip plating and bonding [4], and then obtained by a cold/hot stamping forming [5].

However, due to the difference in physical and chemical properties and formability of dissimilar materials, coordinated deformation of prefabricated laminates is hard to achieve. Therefore, defects such as cracking and rebound are easily generated during forming process. In addition, since the metal bonding process is prone to produce brittle intermetallic compounds [6], the formability in subsequent plastic deformation is further affected, and the stacking sequence is strictly defined. Therefore, due to the lack of flexible deformation mode, the achievable shape of laminated layers is currently limited in further processing steps.

In the aspects of investigations on formability, Mori et al. [7] found that steel and aluminum layers were in different stress states during deep drawing on both sides of the Al/steel laminates. The arrangement of the upper and lower rows has a large influence on the formability. Choi et al. [8] reported that the plastic strain of different laminates was different during the stretching process of the laminated samples, which caused distortion. Hino et al. [9] believed that the rebound amount of laminated layers is affected by various factors such as material strength and thickness, and the difference in material arrangement between inner and outer surfaces will also affect the final rebound amount. Bagherzadeh et al. [10] found that the arrangement of the inner and outer sheets has an effect on formability. Apart from the above studies on bonded laminates, joint performance produced by friction stir is also an important factor affecting formability for the synchronously bonding and deformation process. To investigate the essence of forming mechanism, material flow behavior is the basic but significant intension, which draws continuous concern for the very practical problem of these processes. Investigations on pin-less friction stir welding are particularly focused on this point during the processes due to the great influence in final performance. The flow modes were evaluated analytically and experimentally [11–13]. In an effective physical measurement way, various tracer techniques and microscopic characterization methods were utilized [14]. In recent decades, incremental sheet forming has made remarkable progress in mechanism investigation and practical application due to its high flexibility and formability [15, 16].

Aiming at applying laminated layers in manufacturing more complicated shape, a friction stir-assisted incremental forming with synchronous bonding of dissimilar sheet metals was conducted here. This newly developed forming process relies on the single point incremental sheet forming technology [17] and the pin-less friction stir solid-state bonding process [18]. This process has a combination of advantages of dissimilar materials to improve properties of products and help manufacture energy-saving hybrid structures, which has broad application prospects in meeting the demands from automobile industry, aerospace, and chemical industry by fabricating lightweight hybrid structures with solid-state bonding. Compared with conventional sheet forming processes, the proposed synchronous manufacturing method employs a novel material flow mode with simultaneous forming and solid-state bonding, which can avoid the defects caused by the uncoordinated deformation in conventional forming and the residual stress caused by uneven deformation. In addition, the compressive normal stress in the forming zone obtained by this process can further improve the formability of the sheet. From another perspective, the AA5052-H32 layer not directly in friction contact with the tool can be used as the substrate to microscopically observe the material flow and deformation of the composite Al/steel plate. It is an effective advantage compared with the material tracer methods, which is difficult to implementation in friction stir welding process [14].

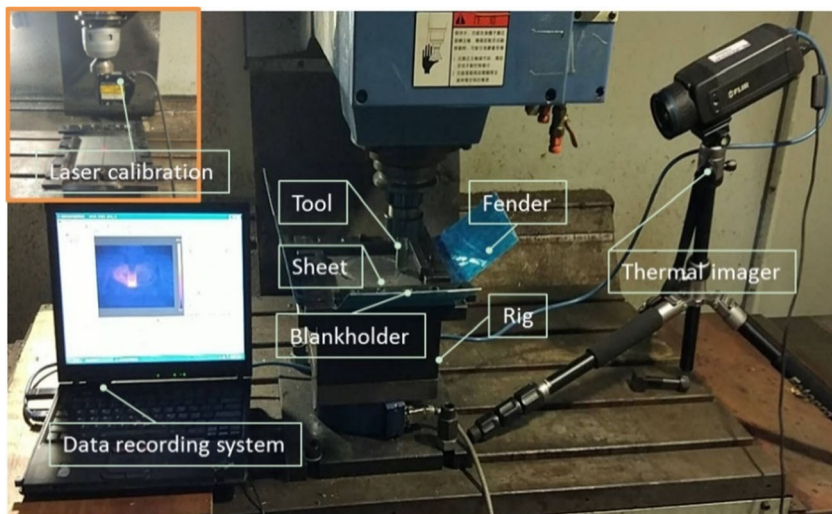
In this work, a concise description of material flow behavior was made in the newly developed FS-ISF&SB process, which provides a better understanding of the underlying material flow mechanism of the process and establishing process window in potential industrial applications. The experimental setup and geometrical design of part are briefly introduced in Sect. 2. Characterizations of material flow in three different zones are made to reveal the macro and microscopic mechanism of this novel process hereafter in Sect. 3. Some concluding remarks are drawn in Sect. 4.

2 Experimental procedures

The incremental forming with synchronous bonding process for multi-field coupling of metal laminates is conducted, the core of which is to superimpose the delaminated dissimilar metal sheets. After removing the surface oxide layer, high pressure and heat generated while conducting incremental forming are applied. During this process, the sheets undergo local plastic deformation and adhesion between the interfaces under the extrusion between forming tool and supporting auxiliary plate. With continuous temperature rising and transferring, the dissimilar layers are finally completely bonded.

Experimental configuration is briefly introduced here. The infrared thermometer high-speed camera sensor is used to measure the temperature during processing. The laser

Fig. 1 Experimental configure and conduction phenomenon



displacement sensor is used to calibrate the local position and overall contour on the workpiece. Figure 1 shows the laser calibration and measurement setting. The synchronous forming process is controlled by CNC machining center. The as-received sheets are stacked by three metal layers: DC05+ AA5052-H32+ DC05, in an order from top to down. Auxiliary plate is placed under the formed laminates to provide sufficient back pressure support. Boron nitride blocker is evenly covered on the contact surface of the lower two layers to avoid soldering. A set of typical and specific process parameters are listed in Table 1. Schematic of designed forming tool and part is shown in Fig. 2. Flat-bottomed with arc-transformed tool can ensure sufficient frictional contact area and also facilitates incremental deformation of local materials.

It is necessary to verify the quality of forming part versus design intent for practical application. In order to characterize material flow modes in different portions, three portions are divided on the radial section. Thermo-mechanical method and electron microscopy solution are taken to characterize material flow behavior. The microstructures of the RFZ were characterized by optical microscope (OM) instrument. Specimen is firstly mechanically polished and then chemically treated using a solution of 4% nitric acid solution (volume ratio) in 90 s. The morphological characterization and thermal

analysis of each region will be introduced one by one in the following subsections.

3 Macro and microscopic mechanism of material flow in FS-ISF&SB

3.1 Assessment of deformation and bonding performance

As shown in Fig. 3a, evaluated portions are located at the wall flow zone (WFZ), rotation flow zone (RFZ), and bump structure flow zone (BSFZ). Different process windows will result in different presentations of the three regions, and some regions will not even appear after improvement, such as BSFZ. Based on the mechanical mechanism of ISF, thickness reduction occurs as usual. Moreover, on the surface of upper layer contacted with high-speed rotational forming tool, the residual scallop exists virally for different toolpath strategies. It is admitted that residual scallop is the main factor to affect surface roughness [19]. Another cause of surface roughness is attributed to the adhesion caused

Table 1 Experimental process parameters setup in the FS-ISF&SB process

Parameters	T_r (°C)	Δh (mm)	ω (rpm)	v (mm/min)
Value	25	0.3	4500	1050

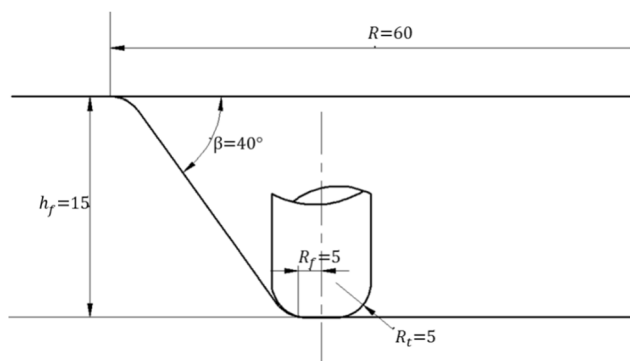


Fig. 2 Schematic of designed part with forming tool (unit: mm)

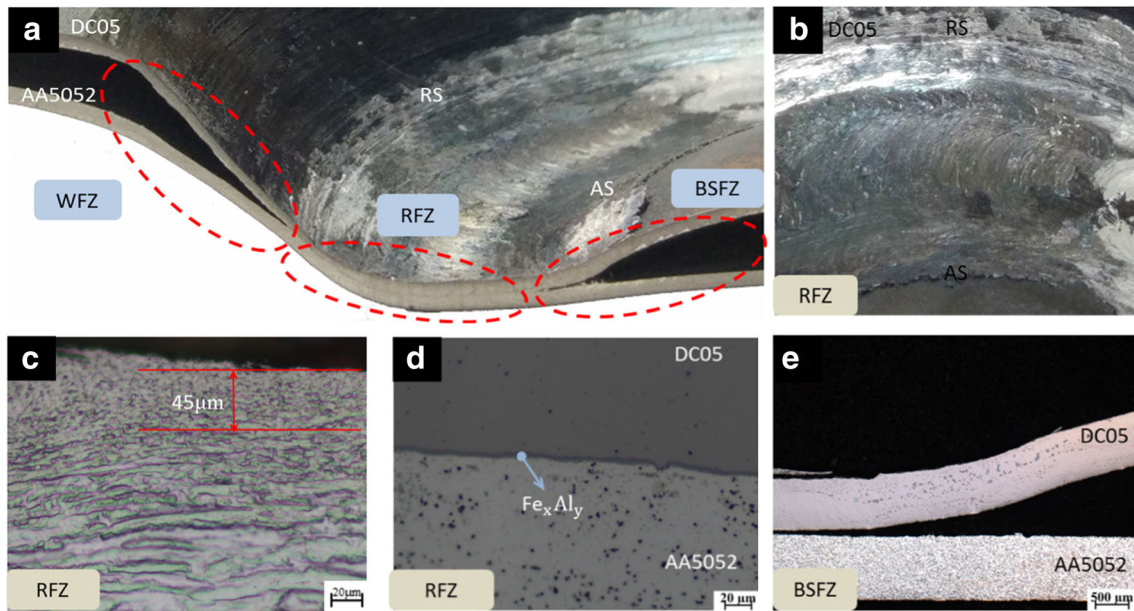


Fig. 3 Illustration of portions in forming part

by the tool with the sheet metal surface as the deforming material undergoes softening under elevated temperature. Figure 3 b shows a typical part by FS-ISF&SB to demonstrate the acceptable inner surface of steel side. Figures 3 c and d provide inner sights of the immediate correlation between forming performance and micro-macro structure evolution. Due to the effect of friction stir, a fine crystal layer of approximately 45- μ m-thick surface is found as shown in Fig. 3c. The intermetallic compounds (Fe_xAl_y) appear at the dissimilar interface as shown in Fig. 3d. A bump structure shape is found by OM as shown in Fig. 3e.

As a dissimilar bonding process, tear strength tests are conducted in a universal tensile testing machine to prove the bonding strength. The average strength of the forming part is 395.75 N by four tests as illustrated in Fig. 4. Under the same process parameters, one reason for the uneven strength should

be the randomness of the generation and growth of the intermetallic compound layer.

The experimental temperature data is recorded and represented in Fig. 5. If the forming height is less than 6 mm, the measured peak temperature rises rapidly, and then reaches a slow rise phase similar to a platform in middle and late stages. The temperature at the end of the forming process is about 600 °C. In the following, the measured temperature shows material flow level during the FS-ISF process. For the sake of engineering simplicity, the gradient difference of the temperature along the thickness direction is ignored in the following subsections.

3.2 Wall flow zone

The WFZ of two layers delaminates and thickness distribution in this zone generally follows the cosine law in incremental

Fig. 4 Tear strength tests for FS-ISF&SB forming process

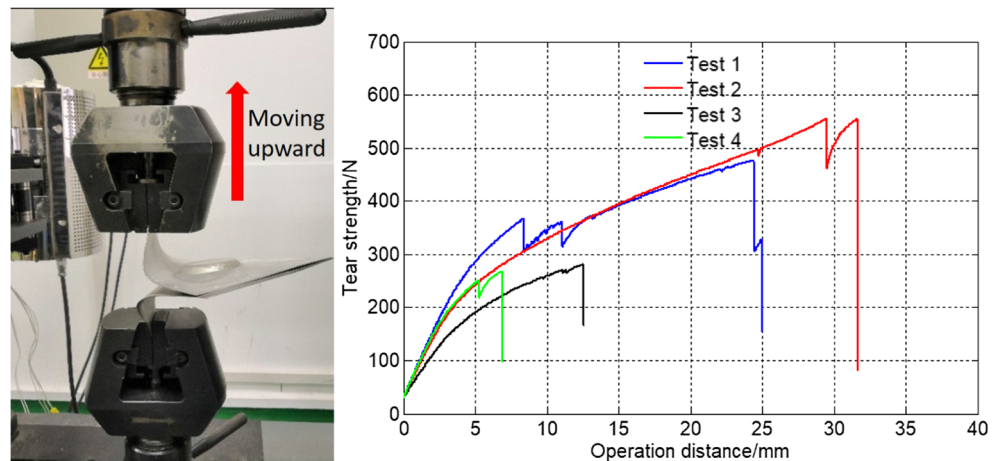
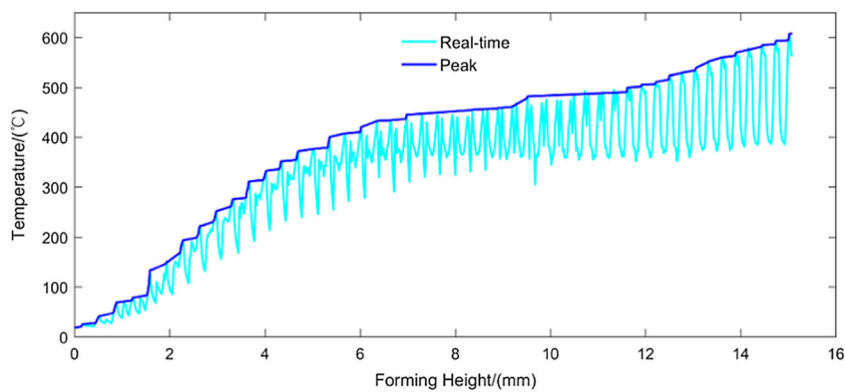


Fig. 5 Temperature record during the FS-ISF&SB forming process



sheet forming. As shown in Fig. 3a, the deformed area shall be bonded as a whole, which, however, differs from the practical appearance. In order to explain this phenomenon, an analytical model is established to evaluate the forming mechanics. Some essential assumptions are made as follows:

- (a) Effects of strain rate and temperature are not considered;
- (b) Bending effect is taken into account for the upper layer and middle layer;
- (c) Influence of torque is neglected at the arc transition zone of forming tool.

Enlightened by the deformation mechanism in ISF [20, 21], membrane method is employed for mechanical analysis of the auxiliary sheet, which only supplies back pressure support for the forming layers. Back pressure distribution in compressive area (see Fig. 6) is obtained as boundary condition for through-thickness normal stress at contact with AA5052-H32 layer, which is solved as

$$\sigma_{tb}^L = \frac{K_U \bar{\epsilon}^n}{(\mu \sin \beta \cdot \theta - 1) \frac{R_t + t_U + t_L}{t_U} - 1} \tag{1}$$

where subscripts U and L denote the upper and lower layers. As a friction-stirred based process, coefficient of friction is quite important. Referred to our previous work in experiments and simulation investigations, friction coefficient is taken as 0.15 here [22]. In plane strain stress state, the equivalent plastic strain converted by the normal strain component can be expressed as

$$\bar{\epsilon} = -\frac{2}{\sqrt{3}} \epsilon_t = \frac{2}{\sqrt{3}} \ln(\sin \beta) \tag{2}$$

Following analytical procedures of force equilibrium equations considering bending effect [23], through-

Fig. 6 Illustration of element stress state and force applied by tool and auxiliary back sheet

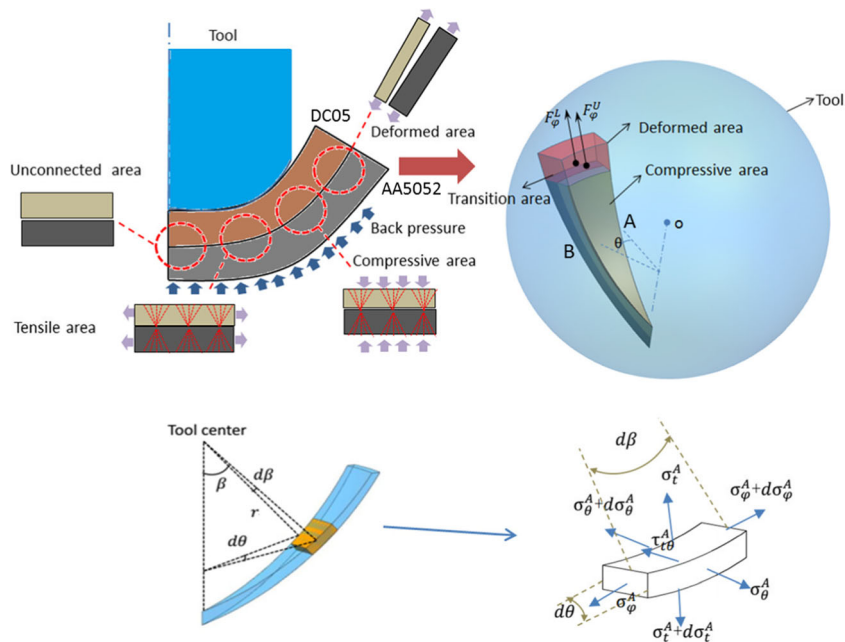


Table 2 Material parameters used in Hollomen’s power law [24]

Material	K (MPa)	<i>n</i> (–)	<i>t</i> ₀ (mm)	<i>ρ</i> (g/cm ³)
DC05	522.6	0.234	0.8	7.70
AA5052-H32	388.6	0.230	1.0	2.75

thickness normal stress is thus obtained for AA5052-H32 layer as a form of differentia function,

$$\frac{d\sigma_t^L}{dr} = \sqrt{3} \frac{\sigma_s^L}{r} \tag{3}$$

where *r* is the distance from the tool center to contact surface as shown in Fig. 6. Integrating the formula and using the boundary condition Eq. (1), the through-thickness normal stress for lower AA5052-H32 layer is obtained as,

$$\sigma_t^L = \sqrt{3} \sigma_s^L \ln \frac{r}{R_t + t_U + t_L} + \sigma_{ib}^L \tag{4}$$

Thus, boundary condition for through-thickness normal stress at contact with upper DC05 layer is deduced as follows,

$$\sigma_{ib}^U = \sqrt{3} \sigma_s^L \ln \frac{R_t + t_U}{R_t + t_U + t_L} + \sigma_{ib}^L \tag{5}$$

Therefore, the compressive normal force *F*_{*t*} in lower and upper layer is given as

$$F_t^L = \int_{-\frac{\theta_0}{2}}^{\frac{\theta_0}{2}} \int_{\beta_0}^{\frac{\pi}{2}} |\sigma_{ib}^L| (R_t + t_U + t_L)^2 \cdot \cos\beta d\beta \cdot \cos\theta d\theta \tag{6}$$

$$F_t^U = \int_{-\frac{\theta_0}{2}}^{\frac{\theta_0}{2}} \int_{\beta_0}^{\frac{\pi}{2}} |\sigma_{ib}^U| (R_t + t_U)^2 \cdot \cos\beta d\beta \cdot \cos\theta d\theta \tag{7}$$

Superscript or subscript *U* and *L* represent the upper layer DC05 or lower layer AA5052-H32, respectively. Under mechanical equilibrium condition of element, the force in the meridian direction is derived as

$$F_\phi = F_t \times \left[\sin \frac{\beta}{2} + \frac{\cos\beta \times \cos \frac{\beta}{2}}{\sin\beta} \right] \tag{8}$$

For the motion coordination consideration of elements in WFZ, a deformation coordination coefficient *V_e* is defined as a factor by comparing stretching force at region A and region B in a unit time domain *dτ* dividing the effect of material density and original sheet thickness *t*₀.

$$V_e = \frac{F_\phi d\tau}{t_0 \rho \theta} \tag{9}$$

where *θ* denotes the circumferential contact angle. Uncoordinated motion of the elements existing in the upper and lower layers in the radial direction is derived from the Eq. (9), which can also derive that incoordination varies with the forming angle. Numerically implemented in the MATLAB coding by using the parameters listed in Table 2, the curves of normalized deformation coordination coefficient versus forming angle can be plotted and compared visually.

Direct evidence of the uncoordinated deformation of the WFZ between the upper and lower layers is represented in Fig. 7. The phenomenon that the dissimilar sheets obviously fail during synchronized forming. In the case, forming angle is less than 10°, good motion uniformity can be maintained between the interfaces, if the angle is larger, uncoordinated separation behavior of the interfaces in the radial direction will cause the layers to fail to complete stable diffusion and create compliant bonding. This is consistent with the actual experimental situation, as shown in Fig. 3a. If the forming angle gets smaller, even approaching zero, then

Fig. 7 Illustration of the element motion states along radial direction

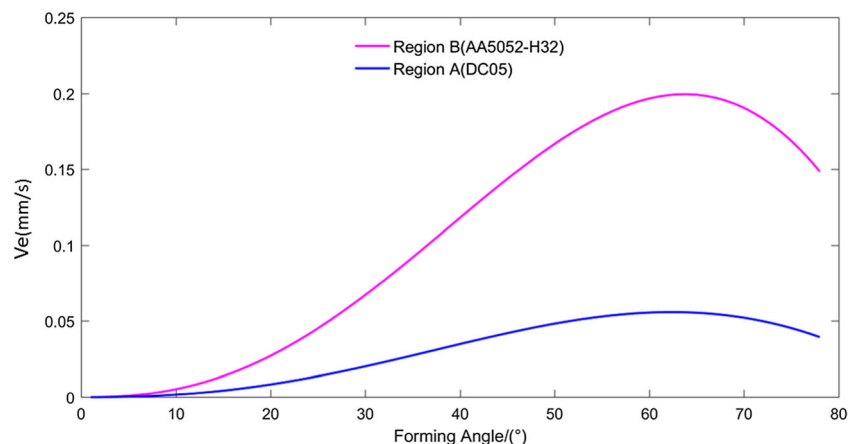
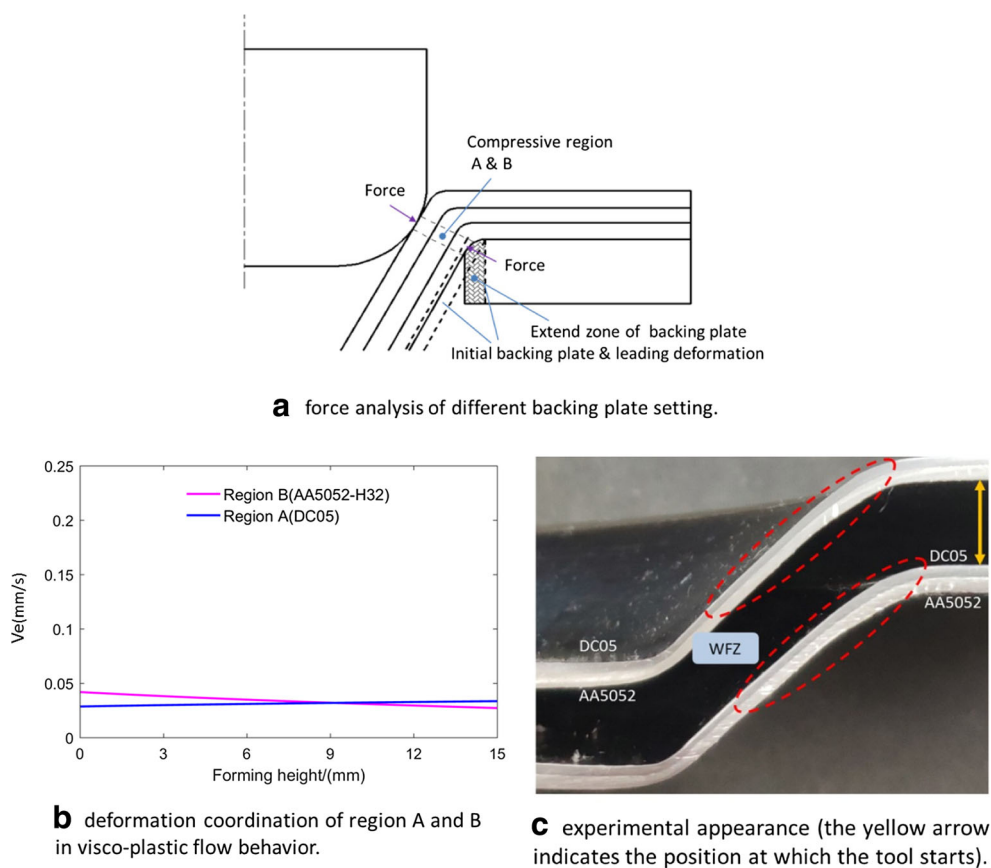


Fig. 8 Illustration of well-deformed part in WFZ



the deformation of regions A and B is relatively synchronous, which is somewhat similar to the case of hot pressure diffusion and the possibility of misalignment between the layers is low. Nevertheless, the response behavior of materials may be more complex under actual conditions, which is affected by multiple physical factors, such as temperature, equipment stability, and sheet anisotropy.

To avoid this undesired phenomenon to be further analyzed in the following sections, it requires a certain time period with high enough temperature to complete the bonding condition to produce joint with reliable structure strength. In order to avoid delamination in the WFZ, deformation coordination of laminated sheet region A and B in meridian direction needs other assistant conditions. Therefore, temperature effect must be acted upon in advance and material in WFZ performs visco-plastic flow behavior. As shown in Fig. 8a, it is possible to keep sufficient contact between these layers

with heat generated in WFZ by back support force. In addition, the starting point fits snugly against the back auxiliary plate to avoid the apparent bending radius (see L1 in Fig. 10). It is also demonstrated in Fig. 8b that predefined temperature (about 160 °C) at initial forming height helps improve the deformation coordination of regions A and B. However, the requirements of backing plate rigidity and consistency of machine are relatively high to avoid delamination of upper and lower layers in WFZ and raise temperature sharply in a short term, which is also another challenge for the equipment system. Therefore, friction stir-assisted double-sided incremental forming is regarded as another alternative solution for obtaining high enough initial temperature.

3.3 Rotation flow zone

The high-speed rotation forming tool contacting with inner layer DC05 provides normal compressive pressure

Table 3 Johnson-Cook model parameters for material AA5052-H32

A (MPa)	B (MPa)	<i>n</i> (–)	<i>C</i> (–)	ϵ_0 (s ⁻¹)	<i>T_r</i> (°C)	<i>T_{melt}</i> (°C)	<i>m</i> (–)
176	325.4	0.5119	0.02	0.1	25	607	0.8557

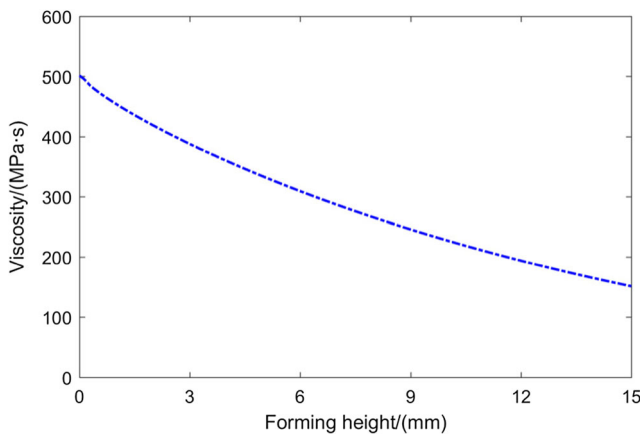


Fig. 9 Calculated viscosity versus forming height

and generates heat and, thus leads diffusion of atoms to form intermetallic bonding between the laminates. Cyclical localized loading conditions show great difference in this process. Since torque conducted by the connection between tool and upper sheet, RFZ is only evaluated in DC05 sheet. For evaluating plastic deformation with high temperature, Johnson-Cook model is employed to express strain rate $\dot{\epsilon}$, work hardening and thermal softening effects, which is written as,

$$\bar{\sigma} = [A + B\bar{\epsilon}^n] \left[1 + C \ln \frac{\dot{\epsilon}}{\dot{\epsilon}_0} \right] \left[1 - \left(\frac{T - T_r}{T_{melt} - T_r} \right)^m \right] \quad (10)$$

Referring to Giuseppina’s method [25], the strain rate $\dot{\epsilon}$ is approximately derived as

$$\dot{\epsilon} = \frac{(1 - \sin\beta)v}{2\pi r_h} \quad (11)$$

The viscosity, which reflects flow flexibility of material [12], is determined from equivalent flow stress and strain rate by using visco-plasticity model [26].

$$\xi = \frac{\bar{\sigma}}{3\dot{\epsilon}}$$

$$= \frac{2\pi r_h [A + B\bar{\epsilon}^n] \left[1 + C \log \frac{\dot{\epsilon}}{\dot{\epsilon}_0} \right] \left[1 - \left(\frac{T - T_r}{T_{melt} - T_r} \right)^m \right]}{3(1 - \sin\beta)v} \quad (12)$$

According to geometric design, r_h is given as Eq. (13), and according to the experimental results, T is also recorded to match forming height in Fig. 5.

$$r_h = R_d - h \sin\beta \quad (13)$$

where h is the current forming height. Submitting parameters listed in Table 1 and Table 3 into Eq. (12), viscosity is then determined by temperature distribution and trajectory circus radius. Both temperature distribution and trajectory circus radius are functions of height position in forming part. Therefore, Fig. 9 is drawn to analytically show the viscosity in different height position in forming part in tangential direction. The obtained viscosity value gets smaller with increase of forming height. Material is subjected to smaller viscous resistance and flow behavior is more pronounced in bottom forming zone, which also matches practical phenomenon in Fig. 10 that deflection occurs on side wall.

In order to track material flow in tangential direction, a black centerline is pre-marked on AA5052-H32 side. At entire forming height (as noted by L_2 in Fig. 10), material in side wall deflects significantly, and linear deflection degree α from the bend to design height could reach 7.2° . Part of the reason is attributed to material properties and spring-back after unloading. The deformation of the L_1 section is caused by the circumferential bending of the sheet and thus loses contact with upper layer, so that this part does not deflect.

Another aspect showing material flow in RFZ is on surface of DC05; as shown in Fig. 3c, a micro surface refined layer is observed in a thickness of about $45 \mu\text{m}$. Torque is not directly applied to sheets through the whole thickness for pin-less friction stir process [27]. Thus, softening caused by temperature and localized working hardening effects are obvious at

Fig. 10 Deflection of side wall in forming part

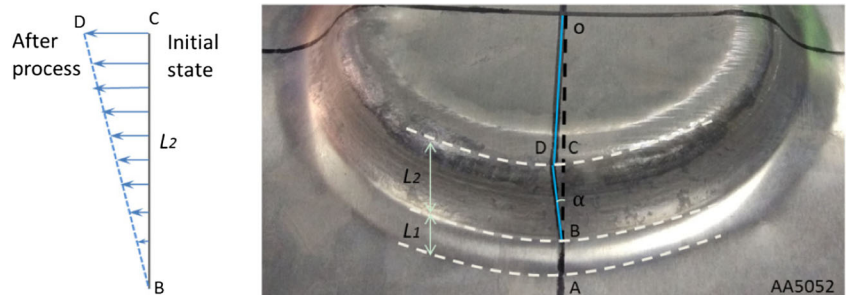
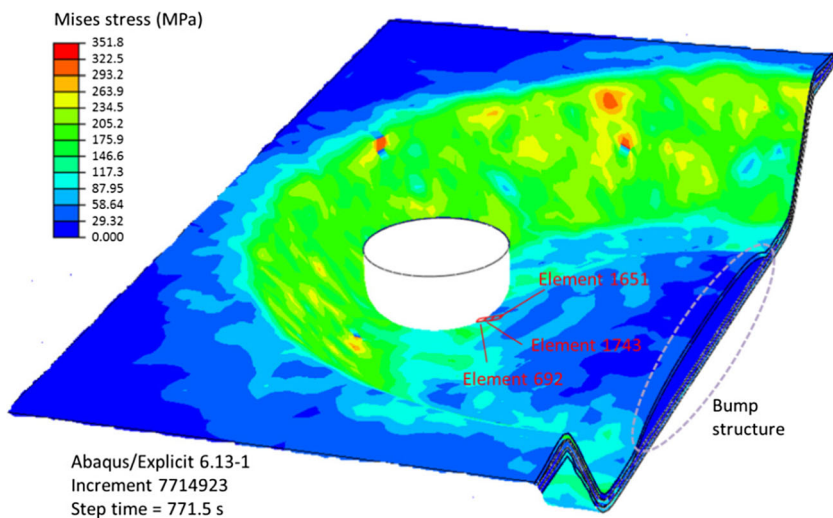


Fig. 11 Sheet deformation by simulation for the FS-ISF&SB process



the outer surface of DC05. Unevenness of deformation causes material accumulation at the arc transition zone of forming tool, which can adversely affect surface quality of DC05 (see Fig. 3b) and it could be optimized by suitable process parameters combination.

3.4 Bump structure flow zone

The processing side where feed velocity vector of forming tool in same direction with rotation velocity vector is named as advancing side (AS) and the opposite direction is called retreating side (RS). As shown in Fig. 3e, material at bottom of DC05 in contact with arc transition zone of forming tool undergoes gradient softening due to temperature effect. Under the push of radial force of forming tool, which moves inward and downward, material gradually flows upward. Bump structure appears in central bottom region of layers and causes geometric errors. On the one hand, the bump structure in this portion gradually accelerates and accumulates as forming tool moving deeper during FS-ISF&SB process. A simulation model was built to make an insight of stress state and deformation response in AS. Shell elements are used in commercial software ABAQUS explicit 6.13 to simulate the material response with thermal-coupled implicit integration algorithm. More details about model setting is referred to our previous work [22]. The focus is paid on an element in the BSFZ here and their positions are represented in Fig. 11. The equivalent strain and stress and equivalent strains in the entire deformation history are plotted in Fig. 12. It can be known from the response history of the tracking element that the equivalent stress originally undergoes work hardening and then experiences heat-induced softening.

Analysis of the whole strain path shows that the deformation tendency of the element located in BSFZ accelerates. The flow behavior of BFSZ boundary element helps to make an insight of this point. The stress components in radial direction are exported as 44.3 MPa and -37.5 MPa of element 692 and 1651, which represents the adjacent elements at the transition of BSFZ. Though through-thickness normal stress cannot be obtained by shell element, as shown in Fig. 13, on the AS, auxiliary plate provides sufficient supporting force and the thrust force caused by radial feed of tool. Thus, resultant force is along the oblique up direction and thus material flow is restricted in radial direction and can only flow in circumferential and thick directions. The element at the transition of BSFZ is subjected to upward buckling deformation, which finally produces bump structure as shown in Fig. 3e.

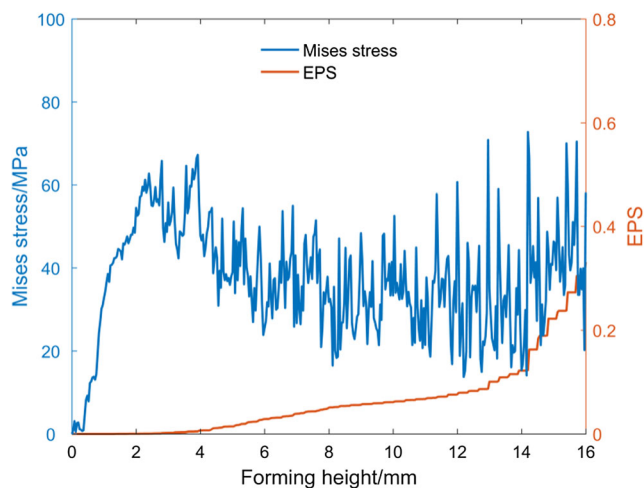


Fig. 12 Equivalent plastic strain and stress response of the selected element 1743 with forming height during forming process by simulation

Fig. 13 Illustration of force conduction and element deformation response at the transition of BSFZ

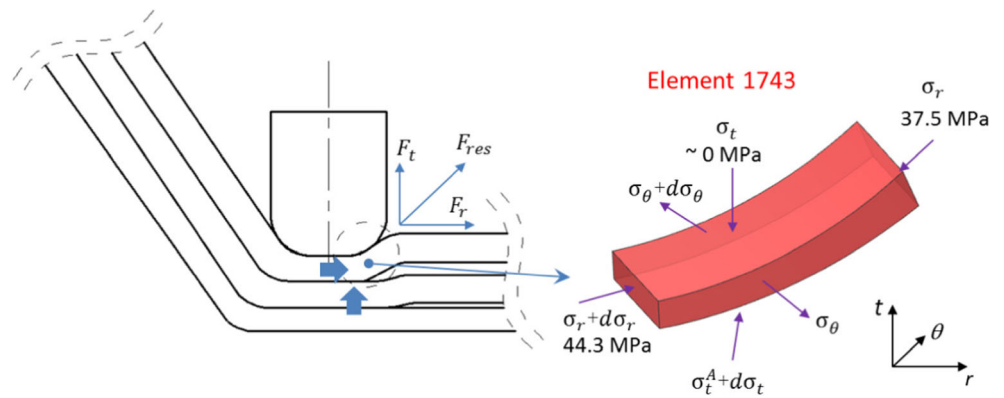
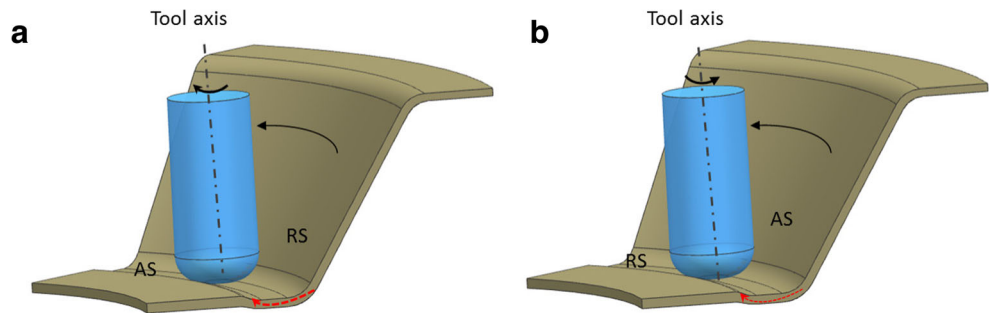


Fig. 14 Illustration of material flow approaching a tool in a ‘climb milling’ method and b ‘up milling’ method



From the mechanical aspect, this bump structure performance can be optimized by changing the direction of tool rotation and other process parameters. The direction of rotation is critical because it is relatively attributed to thermal resultant force. ‘Climb milling’ method and ‘up milling’ method (see Fig. 14) are conducted to evaluate material in this point. The scanned profiles as shown in Fig. 15 indicate that ‘climb milling’ method is beneficial for improving the geometric accuracy in bump shape. It is because tendency of material flow is suppressed in circumferential direction towards unformed bottom zone of DC05 at RS.

The bump structure is a tricky problem for promoting profile accuracy. Such a destabilizing structure is mainly caused by visco-plastic material flow driven by thermal coupled resultant force. Therefore, the combination of the ‘climb-milling’ method with appropriate process parameters, such as the feed rate, rotational speed, step down, and tool path. Thus, it is feasible to carry out optimization in lowering bump structure. This practical point will be the focus of ongoing experimental investigation.

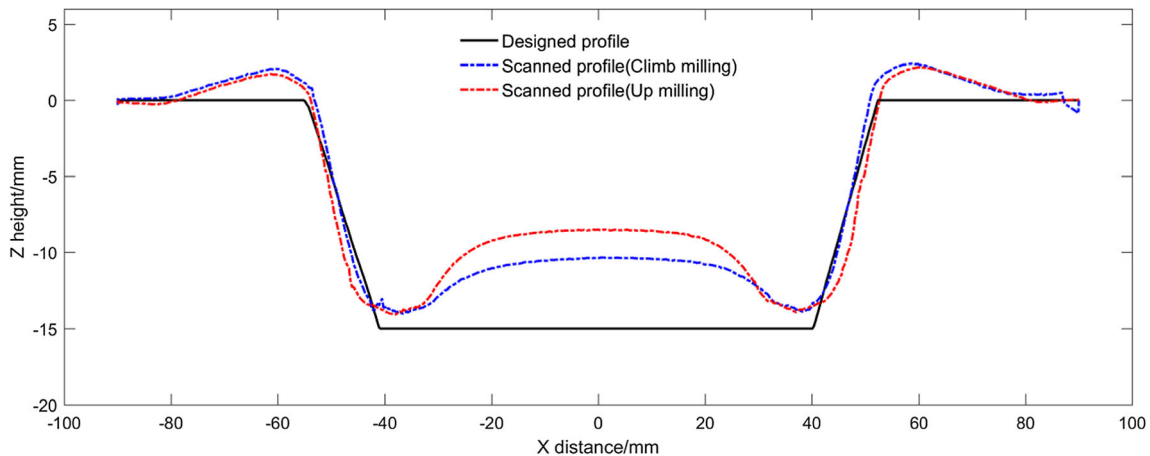


Fig. 15 Contours of designed profile versus forming part profile

4 Concluding remarks

In the present work, characterizations in different material flow zones of FS-ISF&SB process have been made, which makes better understanding of the underlying material flow mechanism of the process and establishing process window in potential industrial applications. Analytical models are developed to illustrate the mechanism of different forming features in three material flow zones. The key conclusions are summarized as follows.

The WFZ is mainly controlled by compressive normal pressure. Due to uncoordinated deformation in meridian direction and low temperature, separation between the upper and lower layers occurs. Increasing of temperature of sheets and back support force in the early process stage is beneficial to ensure solid-state bonding in WFZ.

Increasing heat input in RFZ by friction role shall result in reduced viscosity. Stir friction effect leads material deflecting on the side wall at a linear deflection degree of 7.2° .

The material in connection with arc transition zone of tool on AS results in bump structure (~ 7 mm in height) in BSFZ, which is induced by the resultant of thermal coupled radial and through thickness forces proved by experimental and numerical methods. ‘Climb milling’ method is proved as a useful solution for reducing the height of bump structure for about 3 mm.

For the future work, the effects of anisotropy of sheet layers in forming quality shall be further investigated. In addition, more attentions shall be paid on eliminating the bump structure by pin-less double-sided incremental forming.

Funding information The authors received financial funding from National Natural Science Foundation of China under grant # 51675332 and Program of Shanghai Excellent Academic Research Leadership (19XD1401900).

References

- Chaudhari GP, Acoff V (2009) Cold roll bonding of multi-layered bi-metal laminate composites. *Comp Sci Technol* 69(10):1667–1675
- Parvizi A, Afrouz F (2016) Slab analysis of asymmetrical clad sheet bonded before rolling process. *Int J Adv Manuf Technol* 87(1–4):137–150
- Guo X, Wang H, Liu Z, Wang L, Ma F, Tao J (2016) Interface and performance of CLAM steel/aluminum clad tube prepared by explosive bonding method. *Int J Adv Manuf Technol* 82(1–4):543–548
- Jia J, Zhu WW, Xiong W, Zhou JL (2014) Influence of diffusion ways on morphology of plating layers of hot dip aluminizing stainless steel sample. *Trans Mater Heat Treat* 35:205–209
- Al-Ghamdi KA, Hussain G (2016) On the comparison of formability of roll-bonded steel-Cu composite sheet metal in incremental forming and stamping processes. *Int J Adv Manuf Technol* 87(1–4):1–12
- Bouayad A, Gerometta C, Belkebir A, Ambari A (2003) Kinetic interactions between solid iron and molten aluminium. *Mater Sci Eng A* 363(1–2):53–61
- Yazar Ö, Ediz T, Öztürk T (2005) Control of macrostructure in deformation processing of metal/metal laminates. *Acta Mater* 53(2):375–381
- Choi SH, Kim KH, Oh KH, Dong NL (1997) Tensile deformation behavior of stainless steel clad aluminum bilayer sheet. *Mater Sci Eng A* 222(2):158–165
- Hino R, Goto Y, Yoshida F (2003) Springback of sheet metal laminates in draw-bending. *J Mater Process Technol* 139(1):341–347
- Bagherzadeh S, Mollaei-Dariani B, Malekzadeh K (2012) Theoretical study on hydro-mechanical deep drawing process of bimetallic sheets and experimental observations. *J Mater Process Technol* 212(9):1840–1849
- Cheon J, Yoon JY, Kim C, Na SJ (2018) A study on transient flow characteristic in friction stir welding with real-time interface tracking by direct surface calculation. *J Mater Process Technol* 255:621–634
- Liu XC, Sun YF, Morisada Y, Fujii H (2018) Dynamics of rotational flow in friction stir welding of aluminium alloys. *J Mater Process Technol* 252:643–651
- Mironov S, Masaki K, Sato YS, Kokawa H (2012) Relationship between material flow and abnormal grain growth in friction-stir welds. *Scrip Mater* 67(12):983–986
- Lorrain O, Favier V, Zahrouni H, Lawrjaniec D (2010) Understanding the material flow path of friction stir welding process using unthreaded tools. *J Mater Process Technol* 210(4):603–609
- Behera AK, de Sousa RA, Ingarao G, Oleksik V (2017) Single point incremental forming: an assessment of the progress and technology trends from 2005 to 2015. *J Manuf Process* 27:37–62
- Barnwal VK, Chakrabarty S, Tewari A, Narasimhan K, Mishra SK (2018) Forming behavior and microstructural evolution during single point incremental forming process of aa-6061 aluminum alloy sheet. *Int J Adv Manuf Technol* 95:921–935
- Fang Y, Lu B, Chen J, Xu DK, Ou H (2014) Analytical and experimental investigations on deformation mechanism and fracture behavior in single point incremental forming. *J Mater Process Technol* 214(8):1503–1515
- Bakavos D, Chen Y, Babout L, Prangnell P (2011) Material interactions in a novel pinless tool approach to friction stir spot welding thin aluminum sheet. *Metal Mater Trans A* 42(5):1266–1282
- Ambrogio G, Filice L, Gagliardi F (2012) Improving industrial suitability of incremental sheet forming process. *Int J Adv Manuf Technol* 58(9–12):941–947
- Lu B, Fang Y, Xu DK, Chen J, Ou H, Moser NH, Cao J (2014) Mechanism investigation of friction-related effects in single point incremental forming using a developed oblique roller-ball tool. *Int J Mach Tools Manuf* 85:14–29
- Lu B, Fang Y, Xu DK, Chen J, Ai S, Long H, Ou H, Cao J (2015) Investigation of material deformation mechanism in double side incremental sheet forming. *Int J Mach Tools Manuf* 93:37–48
- Cai S, Wu RH, Wang ZH, Li M, Chen J (2020) Coupled thermo-mechanical modeling of friction stir assisted incremental forming with synchronous bonding of heterogeneous sheet metals. *Int J Adv Manuf Technol* 106:2747–2763
- Ai S, Lu B, Chen J, Long H, Ou H (2017) Evaluation of deformation stability and fracture mechanism in incremental sheet forming. *Int J Mech Sci* 124–125:174–184
- Hollomon JH (1945) Tensile deformation. *Trans AIME* 162:268–290

25. Giuseppina A, Claudio C, Luigino F, Francesco G (2016) Theoretical model for temperature prediction in incremental sheet forming – experimental validation. *Int J Mech Sci* 108-109:39–48
26. Zienkiewicz OC, Corneau IC (2010) Visco-plasticity—plasticity and creep in elastic solids—a unified numerical solution approach. *Int J Num Meth Eng* 8(4):821–845
27. Leon MD, Shin HS (2015) Material flow behaviours during friction stir spot welding of lightweight alloys using pin and pinless tools. *Sci Technol Weld Join* 21(2):140–146

Publisher's note Springer Nature remains neutral with regard to jurisdictional claims in published maps and institutional affiliations.